Informatics in Medicine Unlocked 18 (2020) 100305

Contents lists available at ScienceDirect

Informatics in Medicine Unlocked

journal homepage: http://www.elsevier.com/locate/imu

Automatic classification of cognitively normal, mild cognitive impairment and Alzheimer's disease using structural MRI analysis

V.P. Subramanyam Rallabandi, Ketki Tulpule, Mahanandeeshwar Gattu *, for the Alzheimer's Disease Neuroimaging Initiative[1]

Excelra Knowledge Solutions Pvt. Ltd., Hyderabad, Telangana, India

ARTICLE INFO

Keywords:
Magnetic resonance imaging
Structural atrophy
Cortical thickness
Mild cognitive impairment
Alzheimer's disease
Machine learning

ABSTRACT

Background and objective: Early detection of dementia for clinical diagnosis is challenging due to high subjectivity and individual variability in cognitive assessments, as well as the evaluation of protein biomarkers, which are mostly used for staging of Alzheimer's disease. Currently, although there is no effective treatment for Alzheimer's disease, early detection of dementia through magnetic resonance imaging analysis may assist in developing preventive measures to slow disease progression. In this paper, we developed an automated machine learning method for classifying cognitively normal aging, early mild cognitive impairment, late mild cognitive impairment, and Alzheimer's disease individuals.

Materials and methods: In this study, a total of 1167 whole-brain magnetic resonance imaging scans of individuals who are cognitively normal aging controls, early mild cognitive impairment, late mild cognitive impairment, and patients with probable Alzheimer's disease were obtained from the Alzheimer's Disease Neuroimaging Initiative database. We measured regional cortical thickness of both left and right hemispheres (68 features) using FreeSurfer analysis for each individual, and utilized these 68 features for model building. We further tested scans of individuals to classify them into four groups using various machine learning methods.

Results: We found that the cortical thickness feature, based on the non-linear support vector machine classifier with radial basis function, showed the highest specificity (0.77), sensitivity (0.75), F-score (0.72), Matthew's correlation coefficient (0.71), Kappa-statistic (0.69), receiver operating characteristic area under the curve (0.76), and an overall accuracy of 75% in classifying all four groups using ten-fold cross-validation with respect to the clinical scale. In addition, we also predicted the features for classifying all four groups using the support vector regression algorithm.

Conclusion: The non-linear support vector machine using a radial basis function kernel showed good accuracy in classifying different stages of dementia. Thus, machine learning methods are useful for radiological imaging tasks such as diagnosis, prognosis, risk assessment, and early detection.

1. Introduction

Quantitative non-invasive imaging biomarkers are much needed in clinical diagnosis rather than qualitative imaging biomarkers, since the progression of the neuropathology in Alzheimer's disease (AD) can be observed much earlier before clinical symptoms of the disease become apparent [1]. AD pathology is detectable non-invasively using magnetic resonance imaging (MRI) because of differences in signal intensities of various brain tissues. The MRI biomarker for classifying mild cognitive impairment (MCI) and conversion to AD using manual volumetric measures of hippocampus is still considered to be the gold standard [2]. Although several manual segmentation methods are available, their reliability under test-retest conditions is poor; hence semi-automated and automated methods play a major role in a realistic setting. Machine learning (ML) methods help in high-dimensional data analysis as well as automated classification that can learn complex patterns of structural changes across different imaging modalities. In general, the classification algorithms include feature extraction, training features to classify, and building predictive models that are useful not only as clinical diagnostic systems but also serve as reliable prognostic markers

* Corresponding author.
E-mail address: nandu.gattu@excelra.com (M. Gattu).

[1] Membership of the Alzheimer's Disease Neuroimaging Initiative can be found in the Acknowledgments section.

https://doi.org/10.1016/j.imu.2020.100305
Received 4 December 2019; Received in revised form 4 February 2020; Accepted 20 February 2020
Available online 27 February 2020

[3]. Furthermore, ML classification frameworks can be used to develop imaging markers or indices by training the multi-dimensional features of an individual subject or patient-specific features with high sensitivity and specificity. Thus, individualized or patient-specific feature-based classification systems are of vital importance in the current age of personalized medicine, as they leverage complex computational processes in addition to considering the genetic or life-style risks [4].

Several supervised and semi-supervised MRI studies have been proposed for classifying AD from cognitive normal aging individuals (CN) in previous reports [5–8]. Also, several studies have reported classifying stable MCI (sMCI) and progressive MCI (pMCI) individuals using semi-supervised methods [9–11], or a combination of support vector machine (SVM) and particle swarm optimisation [12], or other methods such as multi-domain transfer learning [13], random forest classifier [14], partial least square [15] using temporal lobe thickness, hippocampal shape, texture and volumetry [16]. One study demonstrated an accuracy of 96.5% in classifying CN from mild AD by analysing the whole-brain gray matter and temporal lobe region [17]. The same study reported an accuracy of 91.74% in differentiating pMCI from CN and 88.99% in classifying pMCI versus sMCI with only two anatomical regions, namely, amygdala and hippocampus [17]. On the other hand, a recent report showed a classification accuracy up to 59.1% with only two features, left and right hippocampal subiculum using ensemble support vector machine classifier [18]. Furthermore, a surface-based morphometry study classified AD from CN with 87.1% sensitivity and 93.3% specificity [19].

The recent research on computer-aided diagnostic systems in neuroimaging for the classification of prodromal stage such as early MCI (eMCI) and late MCI (lMCI) from AD has attracted exploration of the potential use of MRI in detection at an earlier stage for clinical diagnosis. However, the existing studies have several caveats such as small sample size and variability in image acquisition parameters across various MRI scanners, thereby establishing a need for generalizability and reproducibility irrespective of the scanner or heterogeneity in the patient population. Motivated by different AD/MCI/CN classification studies, we obtained multiple cortical thickness measures from structural MRI scans by automated segmentation techniques for CN, eMCI, lMCI and AD groups as training features, and classified using the ML algorithm. We also highlight the features in classification of CN versus AD and eMCI versus lMCI using the support vector regression algorithm and report the specificity, sensitivity, and classification accuracy rates.

2. Materials and Methods

2.1. Study participants

In this study we used the Alzheimer's Disease Neuroimaging Initiative (ADNI) dataset consisting of different protocols (ADNI-1, ADNI-2 and ADNI-GO). ADNI recruited individuals from multiple sites in United States of America and has collated 1167 scans of adults aged between 55 and 90, consisting of cognitively normal older persons, individuals with early or late MCI, and individuals with early AD. The demographic details of the subjects used in this study were given in Table 1.

2.2. MRI acquisition

T1-weighted MRI images were acquired on 1.5 T Siemen's machine using MP-RAGE sequence with repetition time (TR) = 2730 ms, echo time (TE) = 3.43 ms, Inversion time (TI) = 1000 ms, flip angle (FA) = 7° with 128 sagittal slices typically 256 × 256 matrix with the voxel size of approximately 1.33 mm × 1 mm × 1 mm). The complete details of the imaging protocols, test scores including cognitive scales (i.e. MMSE: Mini-Mental State Examination, range 0–30) and clinical scale, Clinical Dementia Rating (CDR) scale of 0, 0.5, 1, 2 and 3 for healthy controls, mild cognitive impairment, mild AD, moderate AD and severe AD, respectively, are available on the portal (http://adni.loni.usc.edu/).

Table 1
Demographic information about the participant of the study.

Group	Controls (n = 371 scans)	Early MCI (n = 328 scans)	Late MCI (n = 169 scans)	Alzheimer's Disease (n = 284 scans)
Age in Yrs (Mean ± S.D.)	75.68 ± 8.01	72.62 ± 7.33	72.99 ± 7.67)	75.85 ± 7.94
Gender (M: F)	52:48	64.5:35.5	68:32	52:48
MMSE (Mean ± S.D.)	29.1 ± 0.9	28.4 ± 1.5	27.1 ± 1.9	23.4 ± 2.1
CDR Sum of Boxes (Range)	0 to 0.5	0.5 to 2.5	2.5 to 4.5	4.5 to 9
CDR Global Score	0.0 ± 0.0	0.5. ± 0.0	0.5 ± 0.2	0.7 ± 0.3

2.3. Image analysis

We initially extracted the brain tissue from skull stripping using the open source FMRIB's software library (FSL) available at https://fsl.fmrib.ox.ac.uk/fsl/fslwiki/with the brain extraction tool, BET [20]. Then we used the FSL-FAST4 (FMRIB's Automated Segmentation Tool) for 3D-image segmentation of the brain into different tissue types (gray matter, white matter, and cerebrospinal fluid). Further, we performed correction for spatial intensity variations also known as bias field (or radiofrequency inhomogeneities). The underlying method is based on a hidden Markov random field (HMRF) model and an associated Expectation-Maximization algorithm. The whole process is iterative, fully automated, and can also produce a bias field-corrected input image and a probabilistic and/or partial volume tissue segmentation. This method is reliable and robust in comparison to other finite mixture model-based methods that are sensitive to noise. The entire schema is given in Fig. 1.

2.4. Feature extraction

In order to extract the features from the segmented gray matter tissue, we used FreeSurfer (https://surfer.nmr.mgh.harvard.edu/) to compute the regional cortical thickness (CT) of several anatomical regions [21]. Here, we used the Killiany/Desikan parcellation atlas [22] and measured the cortical thickness (in mm). The rationale behind choosing the regional cortical thickness is based on the biological experimental studies that demonstrated the loss of neurons in some cortical and subcortical regions in dementia and as AD progresses, thereby impacting the regional cortical thickness [23]. Cortical thickness is calculated as the distance between the white matter surface (white–gray interface) and pial surface (gray-CSF interface). We then generate a cortical stats file created by the recon-all command and/or mris_anatomical_stats for each hemisphere (e.g., lh.aparc.stats for left hemisphere) into a table in which each line is a subject and each column is a parcellation. The first row in the lh.aparc.stats file corresponds to a list of the above parcellation region names in the left hemisphere in which the first column of each file is the subject_id. In a similar manner, we generated the rh.aparc.stats file corresponding to the right hemisphere. Next, we merged the CT features of left and right hemispheres for each subject, removed the first column name (subject_id), added column (Class), and assigned the label as CN, eMCI, lMCI and AD for cognitively normal, early MCI, late MCI and AD patients, respectively, based on their cognitive score and clinical scale. This file was saved as. csv file for further use as training and testing datasets. Since the regional cortical thickness measure across 4 groups is continuous, we normalized it between 0 and 1.

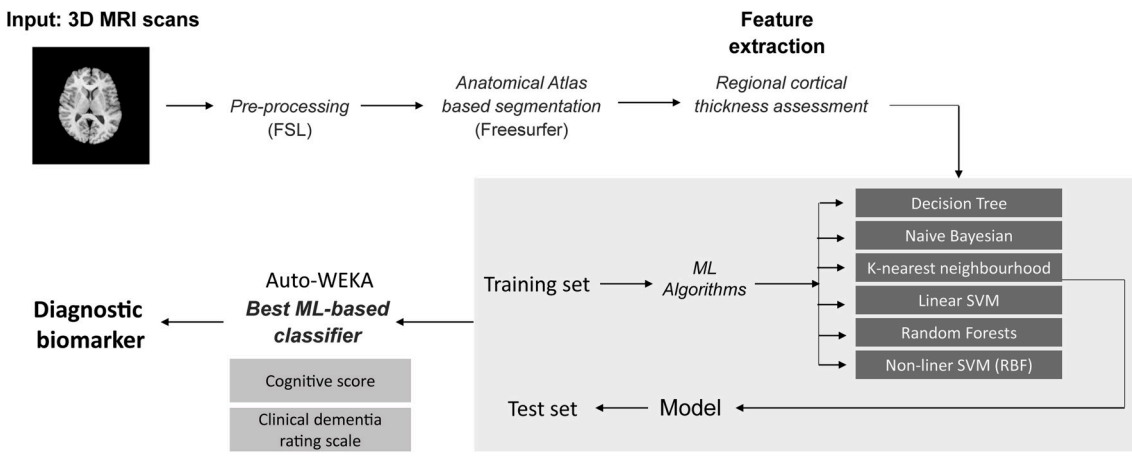

Fig. 1. Schematic diagram of the proposed approach

2.5. Machine learning

We extracted 68 CT features from those regions across all of the four groups of population. These 68 features were trained using several ML algorithms such as naïve Bayesian, *k*-nearest neighbour, random forest, and non-linear support vector machine (SVM) with radial basis function (RBF) kernel using the Auto-WEKA 2.6 tool, which provides a combined algorithm selection and hyper-parameter optimisation over the classification and regression algorithms [24]. Further, we tested on the untrained dataset to predict the group, and validated the classification accuracy based on the cognitive score and clinical scale. We computed the specificity, sensitivity, accuracy, F1-measure, Matthew's correlation coefficient (MCC) and Kappa-statistic with the following formulae:

Specificity = TN / (TN + FP);

Sensitivity (or Recall) = TP/ (TP + FN)

Accuracy = (TP + TN) / (TP + TN + FP + FN)

F1- measure = 2*TP / (2*TP + FP + FN)

MCC= ((Tp*TN-Fp*FN) / ((TP + FP)*(TP + FN)*(TN + FP)*(TN + FN)$^{1/2}$)

Kappa-statistic = (Total_accuracy – Random_accuracy) / (1-Random_accuracy)

where Total_accuracy = (TP + TN) / (TN + TP + FN + FP) and

Random_accuracy = ((FP + TN)*(TN + FN)+(FN + TP)*(FP + TP)) / (TN + TP + FN + FP)^2

where TN, TP, FN and FP represent true negatives, true positives, false negatives and false positives, respectively. The receiver operating characteristic (ROC) area under the curve (AUC) is measured by plotting different thresholds (0–1) of precision on the y-axis and the recall on the x-axis.

3. Results

We computed the CT for all the four groups in both left and right hemispheres for 68 regions such as banks superior temporal sulci, entorhinal, cuneus, frontalpole, caudal anterior cingulate, caudal middle frontal, inferiorparietal, fusiform, inferiortemporal, isthmuscingulate, lateraloccipital, precentral, paracentral, middle temporal, insula, lingual, precuneus, parahippocampal, lateral orbitofrontal, medial orbitofrontal, parsopercularis, parstriangularis, parsorbitalis, pericalcarine, posterior cingulate, rostral anterior cingula, postcentral, superiorfrontal, supramarginal, temporal pole, superior parietal, rostral middle frontal, superior temporal and transverse temporal structures as given in Table 2.

The SVM-based regression algorithm predicted 22 CT features for both left and right hemisphere such as caudal anterior cingulate, enthorhinal, inferior temporal, insula, middle temporal, parahippocampal, precuneus, posterior cingulate, superior temporal, temporal pole, left superior frontal and left banks superior temporal sulci in classifying the AD group when compared to NC and other demented groups. Also, the algorithm predicted 32 CT features in classifying lMCI from AD in both left and right hemispheres such as banks superior temporal sulci, caudal anterior cingulate, enthorhinal, frontal pole, fusiform, inferior temporal, insula, middle temporal, pars trangularis, precuneus, superior frontal, temporal pole including left lateral occipital, left parahippocampal, right inferioparietal, right pericalcarine, right posterior cingulate, right rostral middle frontal, right superior temporal and right supramarginal regions. Furthermore, 17 CT features were predicted in classifying eMCI from NC in both left and right hemispheres such as inferior temporal, caudal anterior cingulate, lateral orbitofrontal, precuneus, temporal pole, superior frontal, left cuneus, right enthornial, right fusiform, right parahippocampal and right post central. In addition, ML predicted 22 CT features in classifying eMCI and lMCI in both left and right hemispheres such as fusiform, enthornial, precuneus, insula, parahippocampal, middle temporal, paraopercularis, lateral orbitofrontal, paracentral, right caudal anterior cingulaute, right caudal middle frontal, right frontal pole, right superior parietal, right temporal pole and left lingual.

The above estimated features were initially trained using several ML algorithms with optimized parameters, and then tested on untrained data containing four groups of subjects. We found the best performance for the SVM-based classifier using RBF kernel, with the highest accuracy rate in both two-third training and one-third testing data as well as 10-fold cross-validation (CV). The specificity, sensitivity, accuracy, F1-measure, MCC and Kappa-statistic of 10-fold CV using various classification methods are compared and given in Table 3. We found non-linear SVM using RBF kernel to be the best classifier with hyper parameters C = 100000 and gamma = 0.01 for 10-fold cross-validation with respect to clinical scale, CDR global score. We also noticed highest specificity (0.77), sensitivity (0.75), F-score (0.72), Matthew's correlation coefficient (0.71), Kappa-statistic (0.69), ROC AUC (0.76) and overall 10-fold average accuracy (75%) with this method among all of the four groups.

4. Discussion

Recent studies have reported classification of dementia stages like MCI and AD using multivariate data analysis as well as prediction of dementia stage using ML methods. The main goal in clinical diagnosis is automated classification or prediction of imaging phenotypes (features or patterns) based on the stage of the disease. The whole-brain analysis

Table 2
Cortical thickness of the regions for all the four groups.

Region_name	NC (MEAN)	NC (S.D.)	eMCI (MEAN)	eMCI (S.D.)	lMCI (MEAN)	lMCI (S.D.)	AD (MEAN)	AD (S.D.)
lh_bankssuperiortemporalsulci	2.377209	0.66528	2.374848	0.13825	2.374908	0.14515	2.325693	0.14391
lh_caudalanteriorcingulate	2.724782	0.13695	2.674705	0.14183	2.067668	0.40409	2.449767	0.28043
lh_caudalmiddlefrontal	2.375452	0.14746	2.350697	0.17793	2.377401	0.15091	2.347476	0.25925
lh_cuneus	1.874485	0.14126	1.773883	0.14497	1.615654	0.12745	1.552706	0.30057
lh_entorhinal	3.552927	0.27518	3.484406	0.20057	3.300800	0.30110	3.047445	0.29315
lh_frontalpole	2.474899	0.14698	2.483844	0.19371	2.497235	0.27849	2.451216	0.28274
lh_fusiform	2.774344	0.14428	2.725431	0.14603	2.556818	0.28668	2.450005	0.29116
lh_inferiorparietal	2.276931	0.14909	2.230420	0.18002	2.274476	0.14741	2.251103	0.28733
lh_inferiortemporal	2.675327	0.13677	2.600916	0.12085	2.575412	0.13788	2.501627	0.28659
lh_insula	3.224671	0.14279	3.151563	0.27569	3.074683	0.14947	2.921603	0.41288
lh_isthmuscingulate	2.323767	0.13680	2.324535	0.14069	2.323982	0.14467	2.303303	0.28692
lh_lateraloccipital	2.175591	0.14159	2.147282	0.28183	2.198081	0.28866	2.151266	0.27768
lh_lateralorbitofrontal	2.574789	0.14499	2.524345	0.14899	2.552518	0.27969	2.550938	0.27362
lh_lingual	1.975316	0.14442	2.024401	0.14633	1.951729	0.26105	1.947554	0.26079
lh_medialorbitofrontal	2.451421	0.29785	2.446643	0.28505	2.376288	0.14713	2.351242	0.29265
lh_middletemporal	2.724622	0.13983	2.696810	0.28078	2.551253	0.27799	2.450931	0.27749
lh_paracentral	2.149021	0.27962	2.196711	0.30256	2.123980	0.14284	2.151409	0.29308
lh_parahippocampal	2.924824	0.14226	2.901025	0.30051	2.748826	0.30419	2.648166	0.28831
lh_parsopercularis	2.346143	0.27468	2.338804	0.22493	2.373326	0.14236	2.351770	0.29658
lh_parsorbitalis	2.552881	0.27338	2.549925	0.27976	2.553431	0.27302	2.552404	0.29429
lh_parstriangularis	2.249538	0.28145	2.225218	0.14543	2.294839	0.70346	2.250841	0.28937
lh_pericalcarine	1.649060	0.29342	1.648627	0.29182	1.656874	0.27085	1.651034	0.29021
lh_postcentral	2.046849	0.29371	2.049151	0.29018	2.052480	0.28785	2.049006	0.29287
lh_posteriorcingulate	2.448940	0.29256	2.380239	0.17449	2.352611	0.28095	2.355289	0.26664
lh_precentral	2.348290	0.28863	2.323311	0.13807	2.348603	0.28784	2.347978	0.29635
lh_precuneus	2.175155	0.14837	2.025160	0.14678	1.952480	0.26590	1.849694	0.28576
lh_rostralanteriorcingulate	2.700340	0.28641	2.725132	0.14362	2.752266	0.28809	2.745986	0.28930
lh_rostralmiddlefrontal	2.226212	0.14620	2.223991	0.14708	2.251173	0.28928	2.246279	0.28398
lh_superiorfrontal	2.546890	0.28980	2.474802	0.14251	2.351646	0.30653	2.251684	0.29504
lh_superiorparietal	2.174566	0.14431	2.174332	0.14357	2.150929	0.26738	2.154255	0.28530
lh_superiortemporal	2.784504	0.20827	2.784613	0.19931	2.651798	0.27775	2.648431	0.27439
lh_supramarginal	2.385703	0.20884	2.325179	0.13713	2.354832	0.28366	2.348271	0.29088
lh_temporalpole	3.931561	0.16842	3.835472	0.12143	3.750161	0.28917	3.648474	0.28492
lh_transversetemporal	2.253918	0.28722	2.250565	0.28794	2.250556	0.29185	2.247889	0.28849
rh_bankssuperiortemporalsulci	2.524291	0.14121	2.524849	0.14924	2.497635	0.29943	2.548462	0.29886
rh_caudalanteriorcingulate	2.675185	0.14690	2.595815	0.28905	2.525104	0.14188	2.448893	0.29285
rh_caudalmiddlefrontal	2.273731	0.14066	2.294851	0.28509	2.250883	0.27418	2.252701	0.27452
rh_cuneus	1.825299	0.14045	1.825111	0.15190	1.826640	0.14703	1.848055	0.27429
rh_entorhinal	3.303551	0.27765	3.251562	0.30251	3.104090	0.58473	2.919943	0.41124
rh_frontalpole	2.475050	0.14347	2.500411	0.29515	2.457839	0.26929	2.496594	0.28729
rh_fusiform	2.624261	0.14193	2.549063	0.28185	2.498964	0.30397	2.401109	0.30246
rh_inferiorparietal	2.350110	0.17892	2.375258	0.14232	2.398760	0.30571	2.348794	0.29950
rh_inferiortemporal	2.743383	0.22801	2.724236	0.14205	2.648730	0.28339	2.572172	0.43231
rh_insula	3.049631	0.29596	3.025561	0.14239	3.051927	0.29028	2.999115	0.28279
rh_isthmuscingulate	2.328788	0.17657	2.324529	0.14392	2.352343	0.28003	2.351731	0.27302
rh_lateraloccipital	2.130567	0.173967	2.149599	0.296196	2.151824	0.29540	2.145597	0.28685
rh_lateralorbitofrontal	2.631764	0.17770	2.624764	0.14554	2.652809	0.27401	2.651663	0.27948
rh_lingual	1.929951	0.17630	1.925006	0.15183	1.936649	0.23006	1.944797	0.25388
rh_medialorbitofrontal	2.547414	0.28629	2.524699	0.14738	2.553418	0.28954	2.548271	0.29242
rh_middletemporal	2.727210	0.17837	2.703006	0.29581	2.613479	0.20177	2.548392	0.28428
rh_paracentral	2.298909	0.28321	2.324358	0.14427	2.272681	0.13481	2.251105	0.28721
rh_parahippocampal	2.689312	0.22589	2.548527	0.29097	2.452122	0.28649	2.451685	0.29482
rh_parsopercularis	2.333495	0.20587	2.328135	0.17998	2.347007	0.28635	2.349732	0.29255
rh_parsorbitalis	2.545918	0.21844	2.575254	0.13274	2.554157	0.27978	2.553045	0.28057
rh_parstriangularis	2.339862	0.22441	2.373892	0.14586	2.397546	0.27739	2.346481	0.27358
rh_pericalcarine	1.676255	0.14708	1.650323	0.30856	1.696729	0.28961	1.649579	0.28608
rh_postcentral	2.151012	0.28790	2.124752	0.14398	2.174932	0.14759	2.148653	0.28970
rh_posteriorcingulate	2.254184	0.27689	2.198916	0.28512	2.050465	0.28000	2.000076	0.28168
rh_precentral	2.350153	0.28163	2.386776	0.19451	2.350895	0.29240	2.352488	0.28865
rh_precuneus	2.275249	0.14634	2.176142	0.13839	2.050403	0.29530	1.940692	0.22906
rh_rostralanteriorcingula	2.853524	0.28883	2.897321	0.29409	2.852346	0.27641	2.849065	0.28970
rh_rostralmiddlefrontal	2.174736	0.14294	2.174766	0.14444	2.199224	0.27882	2.148415	0.29503
rh_superiorfrontal	2.531151	0.18089	2.518936	0.11337	2.500411	0.28790	2.549767	0.28289
rh_superiorparietal	2.083333	0.40823	2.151650	0.29272	2.075238	0.14410	2.053853	0.28296
rh_superiortemporal	2.740806	0.23541	2.624589	0.14609	2.552970	0.28658	2.044957	0.28561
rh_supramarginal	2.453947	0.28004	2.449300	0.29064	2.498704	0.28047	2.449453	0.28373
rh_temporalpole	3.679370	0.40897	3.500146	0.30352	3.351091	0.30672	3.249179	0.28662
rh_transversetemporal	2.250748	0.26720	2.250908	0.28236	2.252978	0.28060	2.252315	0.29668

and multivariate analysis studies reported significant changes in the hippocampus, putamen, thalamus, amygdala, pallidum entorhinal and cingulate cortex which are associated with AD [25]. A study on classification of early MCI from elderly healthy aging individuals using only two anatomical structures, amygdala and hippocampus, in both hemispheres showed the highest accuracy of up to 0.9 [25]. Surface morphometry of medial temporal lobe structures like hippocampus and entorhinal cortex may be superior to volumetric assessment in predicting conversion to AD in patients clinically diagnosed with MCI [26,27]. Recent MRI studies have been reported to classify MCI and AD patients

Table 3
Comparison of various metrics for different ML methods.

Specificity	Sensitivity	F1-score	Overall Accuracy	MCC	ROC AUC	Kappa-statistic	ML Method
0.77	0.75	0.72	0.75	0.71	0.76	0.69	Non-linear SVM (RBF kernel)
0.69	0.67	0.64	0.68	0.62	0.676	0.61	Naive Bayesian
0.72	0.71	0.67	0.7	0.64	0.697	0.63	K-Nearest Neighborhood
0.74	0.73	0.69	0.73	0.66	0.712	0.65	Random Forest
0.68	0.72	0.66	0.7	0.63	0.697	0.63	Decision Tree
0.75	0.73	0.7	0.74	0.68	0.732	0.67	Linear SVM

from elderly aging normal individuals [28] as well as to predict the patients who may convert from MCI to AD [29,30]. However, differences between early MCI and heathy aging controls are not very evident.

The longitudinal studies for classifying healthy controls, MCI and AD including conversion from one stage to another using hippocampus surface volumes and whole brain analysis, with reported accuracy of up to 0.87 [31] and another study reported the importance of hippocampal local surface marker [32]. The relationship between the entorhinal changes and changes in memory performance suggested that non-AD mechanisms in AD-prone areas may still be causative for cognitive reductions [33]. Other studies have reported that several cortical and subcortical regions including the hippocampus show improved predictive rate [8] while a report on whole-brain gray matter analysis with a deformation-based algorithm showed the best prediction outcome [17]. Various predictive models based on MRI features for slow and fast progression of MCI to AD have been developed, such as the multiple kernel learning model [34], convolutional neural network, and SVM methods [35–37]. Interestingly, our prediction results and accuracy are consistent with an independent recent study reporting MRI based classification with neuropathological AD using ML algorithms such as RF and SVM classifiers with 77% accuracy, corresponding to the anatomical structures such as fusiform, entorhinal, insular cortices, anterior cingulate gyrus both rostral and caudal, and the subcortical regions anterior corpus callosum including lacunar changes in pallidum and inferior putamen [38].

Most of the predictive features of our model were consistently reported in previous studies that are associated with either MCI or AD. The entorhinal cortical thickness, anterior cingulate cortical thickness in rostral and caudal regions were shown to be the best predictors, and both are considered as early markers for AD [39]. Also, a recent pre-mortem MRI study found the entorhinal cortical thickness measure to be strongly correlated with neurofibrillary tangles based on post-mortem AD neuropathological assessment [40]. Previously, a whole-brain MRI analysis study showed an overall accuracy of 94.5% in classifying AD and control subjects using the SVM classifier [41]. A novel two-stage modelling approach achieved an overall prediction accuracy of approximately 80% in classifying MCI, AD, and controls from multiple assessment domains simultaneously, such as cognition, function, fluid biomarkers, brain imaging, and diagnosis of individuals [42].

The proposed imaging biomarker showed a higher false positive rate for classifying late MCI and AD implying a challenge in reflecting the pathological characteristics using FSL and Freesurfer automated methods. However, there are no reliable biomarkers for classifying early MCI and late MCI stages with good accuracy. A recent study reported improved classification accuracy of cognitively normal and MCI (AUC to be 0.78) if APOE4 including cognitive and MRI variables are selected [43]. The prediction performance across 10-fold nested cross-validation using a non-linear radial basis kernel function improved the predictive power of our algorithm. Nevertheless, validation in independent and larger dataset samples is necessary to prove the performance of the model beyond our dataset. Furthermore, a recent study reported that the prediction of AD using SVM and RF algorithms based on MRI features are well-correlated with the autopsy verified neuropathological changes in AD [38]. Also, our results and classification accuracy with nonlinear SVM model corroborates with these results. Another important advantage of our study is the use of multicentric data for analysis on above 1000 individual MRI scans collected on various MRI scanners across multiple sites. A recent multicentric MRI study wherein the spatial position of features and their distribution around the patient's brain were used as input, demonstrated the robustness of this method to automatically classify AD using the SVM method with a good accuracy of about 77%, despite using data from two different imaging datasets [44]. In addition, another recent report showed the feasibility of estimating the AD risk factor across multiple datasets using an anatomical index, AD pattern similarity score, by applying a high-dimensional ML approach [45].

There are few methodological limitations in the existing studies for their application in clinical diagnosis based on ML due to lack of neuropathological correlates with MRI phenotypes, which is the gold standard for the diagnostic decision support system. On the other hand, prediction of the disease progression or conversion from one stage to other needs longitudinal data analysis. The main advantage of the proposed method in the clinical setting is that a model with high accuracy as well as specificity in classifying disease stage is helpful, rather than using cumbersome higher dimensional image processing methods. The disease characteristics may vary case-to-case in the staging of AD like mild, moderate and severe to reflect the neuropathological changes that are correlated with clinical symptoms. To date, no early imaging biomarker for AD is available with strong neuropathologic correlates. Thus, early detection of anatomical changes at the prodromal stage prior to becoming clinically evident may be helpful for preventive measures and designing effective treatment to arrest disease progression.

5. Conclusion

To conclude, we developed a model for early prediction and classification of MCI and AD from elderly cognitively normals, as well as for distinguishing early and late MCI individuals. Of all the algorithms that we tested, non-linear SVM classifier using a radial basis function kernel showed the highest specificity, sensitivity, F-score, MCC and kappa-statistic, ROC AUC including an overall accuracy of 75% for 10-fold cross-validation. The performance of this model may not be useful for clinical diagnosis, but represents a decisive step towards classification of MCI and AD. Thus, the advances in both imaging and machine learning have in tandem led to their potential use in several radiological imaging tasks, such as diagnosis, prognosis, risk assessment, and early detection.

Ethical statement

Availability of data and materials: The data that support the findings of this study are available online and are cited appropriately. We were involved only in data analysis and methodology and not in any clinical testing.

Funding

The data analysis was funded by Excelra Knowledge Solutions Pvt. Ltd, Hyderabad.

Declaration of competing interest

The authors declare that they have no competing interests.

Acknowledgments

Data used in preparation of this article was obtained from the Alzheimer's Disease Neuroimaging Initiative (ADNI) database (adni.loni.usc.edu). As such, the investigators within the ADNI contributed to the design and implementation of ADNI and/or provided data but did not participate in analysis or writing of this report. The ADNI principal investigator is Michael W. Weiner, MD (Michael.Weiner@ucsf.edu). A complete listing of ADNI investigators can be found at: https://adni.loni.usc.edu/wp-content/uploads/how_to_apply/ADNI_Manuscript_Citations.pdf. Data collection and sharing for this project was funded by the Alzheimer's Disease Neuroimaging Initiative (ADNI (National Institutes of Health Grant U01AG024904) and DOD ADNI (Department of Defense award number W81XWH-12-2-0012). ADNI is funded by the National Institute on Aging, the National Institute of Biomedical Imaging and Bioengineering, and through generous contributions from the following: AbbVie, Alzheimer's Association; Alzheimer's Drug Discovery Foundation; Araclon Biotech; BioClinica, Inc.; Biogen; Bristol-Myers Squibb Company; CereSpir, Inc.; Cogstate; Eisai Inc.; Elan Pharmaceuticals, Inc.; Eli Lilly and Company; EuroImmun; F. Hoffmann-LaRoche Ltd and its affiliated company Genentech, Inc.; Fujirebio; GE Healthcare; IXICO Ltd.; Janssen Alzheimer Immunotherapy Research & Development, LLC.; Johnson & Johnson Pharmaceutical Research & Development LLC.; Lumosity; Lundbeck; Merck & Co., Inc.; Meso Scale Diagnostics, LLC.; NeuroRx Research; Neurotrack Technologies; Novartis Pharmaceuticals Corporation; Pfizer Inc.; Piramal Imaging; Servier; Takeda Pharmaceutical Company; and Transition Therapeutics. The Canadian Institutes of Health Research is providing funds to support ADNI clinical sites in Canada. Private sector contributions are facilitated by the Foundation for the National Institutes of Health (www.fnih.org). The grantee organization is the Northern California Institute for Research and Education, and the study is coordinated by the Alzheimer's Therapeutic Research Institute at the University of Southern California. ADNI data are disseminated by the Laboratory for NeuroImaging at the University of Southern California.

Appendix A. Supplementary data

Supplementary data to this article can be found online at https://doi.org/10.1016/j.imu.2020.100305.

References

[1] Braak H, Braak E. Frequency of stages of Alzheimer-related lesions in different age categories. Neurobiol Aging 1997;18:351–7.
[2] Westman E, Simmons A, Zhang Y, Muehlboeck J, et al. Multivariate analysis of MRI data for Alzheimer's disease, mild cognitive impairment and healthy controls. Neuroimage 2011;54(2):1178–87.
[3] Shen D, Wu G, Suk H-I. Deep learning in medical image analysis. Annu Rev Biomed Eng 2017;19:221–48.
[4] Habes M, Toledo JB, Resnick SM, Doshi J, Auwera SV, et al. Relationship between APOE genotype and structural MRI measures throughout adulthood in the SHIP population-based cohort. Am. J. Neuroradiol. AJNR 2016;37(9):1636–42.
[5] Zhang D, Shen D. Predicting future clinical changes of MCI patients using longitudinal and multimodal biomarkers. PloS One 2012;7(3):e33182.
[6] Zhang D, Wang Y, Zhou L, Yuan H, Shen D. For the Alzheimer's Disease Neuroimaging Initiative. Multimodal classification of Alzheimer's disease and mild cognitive impairment. Neuroimage 2011;55(3):856–67.
[7] Cho Y, Seong JK, Jeong Y, Shin SY. Individual subject classification for Alzheimer's disease based on incremental learning using a spatial frequency representation of cortical thickness data. Neuroimage 2012;59(30):2217–30.
[8] Westman E, Muehlboeck J, Simmons A. Combining MRI and CSF measures for classification of Alzheimer's disease and prediction of mild cognitive impairment conversion. Neuroimage 2012;62(1):229–38.
[9] Ye DH, Pohl KM, Davatzikos C. Semi-supervised pattern classification: application to structural MRI of Alzheimer's disease. In: Proc. IEEE international workshop on pattern recognition in NeuroImaging (PRNI). IEEE; 2011. p. 1–4.
[10] Filipovych R, Davatzikos C. Semi-supervised pattern classification of medical images:application to mild cognitive impairment (MCI). Neuroimage 2011;55(3):1109–19.
[11] Batmanghelich KN, Ye DH, Pohl KM, Taskar B, Davatzikos C. Disease classification and prediction via semi-supervised dimensionality reduction. In: IEEE international symposium on biomedical imaging: from nano to macro. IEEE; 2011. p. 1086–90.
[12] Yang S-T, Lee J-D, Chang T-C, Huang C-H, Wang J-J, et al. Discrimination between Alzheimer's disease and mild cognitive impairment using SOM and PSO-SVM. Comput. Math. Method. M. 2013. https://doi.org/10.1155/2013/253670. Article ID 253670.
[13] Cheng B, Liu M, Shen D, Li Z, Zhang D. For the Alzheimer's disease neuroimaging initiative. Multi-domain transfer learning for early diagnosis of Alzheimer's disease. Neuroinformatics 2017;15(2):115–32. https://doi.org/10.1007/s12021-016-9318-5.
[14] Moradi E, Pepe A, Gaser C, Huttunen H, Tohka J. For the Alzheimer's Disease Neuroimaging Initiative. Machine learning framework for early MRI-based Alzheimer's conversion prediction in MCI subjects. Neuroimage 2015;104:398–412.
[15] Wang P, Chen K, Yao L, Hu B, Wu X, Zhang J, Ye Q, Guo X. For the Alzheimer's disease neuroimaging initiative. Multimodal classification of mild cognitive impairment based on partial least squares. J. Alzheimers Dis. 2016;54(1):359–71.
[16] Sørensen L, Igel C, Pai A, Balas I, Anker C, Lillholm M, Nielsen M. For the Alzheimer's Disease Neuroimaging Initiative and the Australian Imaging Biomarkers and Lifestyle flagship study of ageing. Differential diagnosis of mild cognitive impairment and Alzheimer's disease using structural MRI cortical thickness, hippocampal shape, hippocampal texture, and volumetry. NeuroImage Clin 2017;13:470–82.
[17] Long X, Chen L, Jiang C, Zhang L, for the Alzheimer's Disease Neuroimaging Initiative. Prediction and classification of Alzheimer disease based on quantification of MRI deformation. PloS One 2017;12(3):e0173372. https://doi.org/10.1371/journal.pone.0173372.
[18] Sørensen L, Nielsen M. For the Alzheimer's Disease Neuroimaging Initiative. Ensemble support vector machine classification of dementia using structural MRI and mini-mental state examination. J Neurosci Methods 2018;302:66–74.
[19] Lee JS, Kim C, Shin J-H, Cho H, Shin D-S, et al. Machine learning-based individual assessment of cortical atrophy pattern in Alzheimer's disease spectrum: development of the classifier and longitudinal evaluation. Sci Rep 2018;8:4161. https://doi.org/10.1038/s41598-018-22277-x.
[20] Smith SM. Fast robust automated brain extraction. Hum Brain Mapp 2002;17:143–55.
[21] Fischl B, Dale AM. Measuring the thickness of the human cerebral cortex from magnetic resonance images. Proc. Natl. Acad. Sci. U.S.A 2000;97:11050–5.
[22] Desikan RS, Segonne F, Fischl B, Quinn BT, Dickerson BC, et al. An automated labeling system for subdividing the human cerebral cortex on MRI scans into gyral based regions of interest. Neuroimage 2006;31:968–80.
[23] Arendt T, Brückner MK, Morawski M, et al. Early neurone loss in Alzheimer's disease: cortical or subcortical? A*cta Neuropathol Commun* 2015;3:10. https://doi.org/10.1186/s40478-015-0187-1.
[24] Kotthoff L, Thornton C, Hoos H, Hutter F, Leyton-Brown K. Auto-WEKA 2.0: automatic model selection and hyperparameter optimization in WEKA. J Mach Learn Res 2017;18(25):1–5.
[25] Fan Y, Batmanghelich N, Clark CM, Davatzikos C, for the Alzheimer's Disease Neuroimaging Initiative. Spatial patterns of brain atrophy in MCI patients, identified via high-dimensional pattern classification, predict subsequent cognitive decline. Neuroimage 2008;39:1731–43.
[26] Davatzikos C, Bhatt P, Shaw LM, Batmanghelich KN, Trojanowski JQ. Prediction of MCI to AD conversion, via MRI, CSF biomarkers, and pattern classification. Neurobiol Aging 2011;32(12). 2322-e19.
[27] Devanand DP, Bansal R, Liu J, Hao X, Pradhaban G, Peterson BS. MRI hippocampal and entorhinal cortex mapping in predicting conversion to Alzheimer's disease. Neuroimage 2012;60(3):1622–9.
[28] Basaia S, Agosta F, Wagner L, Canu E, Magnani G, Santangelo R, Filippi M, for the Alzheimer's Disease Neuroimaging Initiative. Automated classification of Alzheimer's disease and mild cognitive impairment using a single MRI and deep neural networks. NeuroImage Clin 2018;18(2018):101645.
[29] Falahati F, Westman E, Simmons A. Multivariate data analysis and machine learning in Alzheimer's disease with a focus on structural magnetic resonance imaging. J. Alzheimers. Dis 2014;41:685–708.
[30] Luk CC, Ishaque A, Khan M, Ta D, Chenji S, Yang YH, Eurich D, Kalra S. For the Alzheimer's Disease Neuroimaging Initiative. Alzheimer's disease: 3-Dimensional MRI texture for prediction of conversion from mild cognitive impairment. Alzheimers Dement. (Amst) 2018;10:755–63.
[31] Lillemark L, Sorensen L, Pai A, Dam EB, Nielsen M. For the Alzheimer's Disease Neuroimaging Initiative. Brain region's relative proximity as marker for Alzheimer's disease based on structural MRI. BMC Med Imag 2014;14:21.
[32] Platero C, López ME, Tobar MDC, Yus M, Maestu F. Discriminating Alzheimer's disease progression using a new hippocampal marker from T1-weighted MRI: the local surface roughness. Hum Brain Mapp 2019;40(5):1666–76. https://doi.org/10.1002/hbm.24478.
[33] Fjell AM, Westlye LT, Grydeland H, Amlien I, Espeseth T, Reinvang I, Raz N, Dale AM, Walhovd KB. For the Alzheimer disease neuroimaging initiative. Accelerating cortical thinning: unique to dementia or universal in aging? Cerebr Cortex 2014;24(4):919–34.
[34] Collazos-Huertas D, Cárdenas-Peña D, Castellanos-Dominguez G. Instance-based representation using multiple kernel learning for predicting conversion to

Alzheimer disease. Int J Neural Syst 2018;20:1850042. https://doi.org/10.1142/S0129065718500429.
[35] Li Y, Jiang J, Shen T, Wu P, Zuo C. Radiomics features as predictors to distinguish fast and slow progression of mild cognitive impairment to Alzheimer's disease. Conf. Proc. IEEE Eng. Med. Biol. Soc. 2018:127–30.
[36] Lin W, Tong T, Gao Q, Guo D, Du X, Yang Y, Guo G, Xiao M, Du M, Qu X. For the Alzheimer's Disease Neuroimaging Initiative. Convolutional neural networks-based MRI image analysis for the Alzheimer's disease prediction from mild cognitive impairment. Front Neurosci 2018;12:777.
[37] Shen T, Jiang J, Li Y, Wu P, Zuo C, Yan Z. Decision supporting model for one-year conversion probability from MCI to AD using CNN and SVM. Conf. Proc. IEEE Eng. Med. Biol. Soc. 2018:738–41.
[38] Kautzky A, Seiger R, Hahn A, Fischer P, Krampla W, Kasper S, Kovacs GG, Lanzenberger R. Prediction of autopsy verified neuropathological change of Alzheimer's disease using machine learning and MRI. Front Aging Neurosci 2018; 10:406. https://doi.org/10.3389/fnagi.2018.00406.
[39] Salvatore C, Battista P, Castiglioni I. Frontiers for the early diagnosis of AD by Means of MRI brain imaging and support vector machines. Curr Alzheimer Res 2016;13:509–33.
[40] Thaker AA, Weinberg BD, Dillon WP, Hess CP, Cabral HJ, Fleischman DA, et al. Entorhinal cortex: antemortem cortical thickness and postmortem neurofibrillary tangles and amyloid pathology. Am. J. Neuroradiol. AJNR 2017;38:961–5.
[41] Magnin B, Mesrob L, Kinkingnéhun S, Pélégrini-Issac M, Colliot O, Sarazin M, Dubois B, Lehéricy S, Benali H. Support vector machine-based classification of Alzheimer's disease from whole-brain anatomical MRI. Neuroradiology 2009;51 (2):73–83.
[42] Iddi S, Li D, Aisen PS, Rafii MS, Thompson WK, Donohue MC. Alzheimer's disease neuroimaging initiative. Predicting the course of Alzheimer's progression. Brain Inform 2019;6(1):6.
[43] Albert M, Zhu Y, Moghekar A, Mori S, Miller MI, Soldan A, Pettigrew C, Selnes O, Li S, Wang M-C. Predicting progression from normal cognition to mild cognitive impairment for individuals at 5 years. Brain 2018;141(3):877–87.
[44] Previtali F, Bertolazzi P, Felici G, Weitschek E. A novel method and software for automatically classifying Alzheimer's disease patients by magnetic resonance imaging analysis. Comput Methods Progr Biomed 2017;143:89–95. https://doi.org/10.1016/j.cmpb.2017.03.006.
[45] Casanova R, Barnard RT, Gaussoin SA, Saldana S, Hayden KM, et al. Using high-dimensional machine learning methods to estimate an anatomical risk factor for Alzheimer's disease across imaging databases. Neuroimage 2018;183:401–11.